

Origin of magnetic frustration in $\text{Bi}_3\text{Mn}_4\text{O}_{12}(\text{NO}_3)$

Mojtaba Alaei,^{1,*} Hamid Mosadeq,² Ismail Abdolhossaini Sarsari,¹ and Farhad Shahbazi^{1,†}

¹*Department of Physics, Isfahan University of Technology, Isfahan 84156-83111, Iran.*

²*Department of Physics, Shahrekord University, Shahrekord, Iran*

(Dated: February 20, 2017)

$\text{Bi}_3\text{Mn}_4\text{O}_{12}(\text{NO}_3)$ (BMNO) is a honeycomb bilayers anti-ferromagnet, not showing any ordering down to very low temperatures despite having a relatively large Curie-Weiss temperature. Using *ab initio* density functional theory, we extract an effective spin Hamiltonian for this compound. The proposed spin Hamiltonian consists of anti-ferrimagnetic Heisenberg terms with coupling constants ranging up to third intra-layer and forth inter-layer neighbor. Performing Monte Carlo simulation, we obtain the temperature dependence of magnetic susceptibility and so the Curie-Weiss temperature and find the coupling constants which best matches with the experimental value. We discover that depending on the strength of the second neighbor interlayer exchange J_{2c} , there are two collinear ground states competing each other for this system. In both states, the spin ordering in each layer is Néel type, however for small J_{2c} the nearest neighbor spins in the two layers are antiparallel, while for large J_{2c} they are parallel. Classical Monte Carlo simulation and density matrix renormalization group calculations confirm that exchange couplings obtained for BMNO are in such a way that put this material in a vicinity of a critical point, where the trading between these two ground states prevent it from setting in a magnetically ordered state.

PACS numbers: 71.15.Mb, 75.50.Ee, 75.40.Mg.

$\text{Bi}_3\text{Mn}_4\text{O}_{12}(\text{NO}_3)$ (BMNO) is an experimental realization of frustrated honeycomb magnetic materials, synthesized by Smirnova *et al* [1]. In this compound, the magnetic lattice can be effectively described by a weakly coupled honeycomb bilayers of Mn^{+4} ions (Fig. 1). The temperature dependence of magnetic susceptibility of BMNO does not indicate any ordering down to $T = 0.4\text{K}$, in spite of the Curie-Weiss temperature $\theta_{\text{CW}} \approx -257\text{K}$ [1, 2]. The absence of long-range ordering in BMNO is also confirmed by specific heat measurements [1, 2], neutron scattering [3] and high-field electron-spin relaxation (ESR) experiments [4].

So far, the theoretical attempts to explain the magnetic properties of BMNO have been focusing on the frustration effect of second intra-layer coupling J_2 or the tendency toward dimerization by considering a large anti-ferromagnetic inter-layer nearest neighbor coupling J_{1c} [5–12]. In this paper, we obtain a Heisenberg spin Hamiltonian for BMNO, using an *ab initio* LDA+U calculation. In our calculations, we consider a detailed analysis of nonidentical Mn atoms which were assumed to be identical in the previous calculation [5]. We show that how this consideration can affect the exchange couplings in the spin Hamiltonian. We find that in contrary to the previous works, none of J_2 and J_{1c} are large enough to frustrate BMNO to reach an ordered state. Instead, it is the second neighbor inter-layer coupling J_{2c} which has a crucial role in determining the magnetic properties of this compound.

Ab initio method. To derive magnetic exchange couplings, we employ Density Functional Theory (DFT) with Full-Potential Local-Orbital minimum-basis (FPLO), using FPLO code [13] (FPLO14.00-45). For charge analysis we employ Projector Augmented Wave

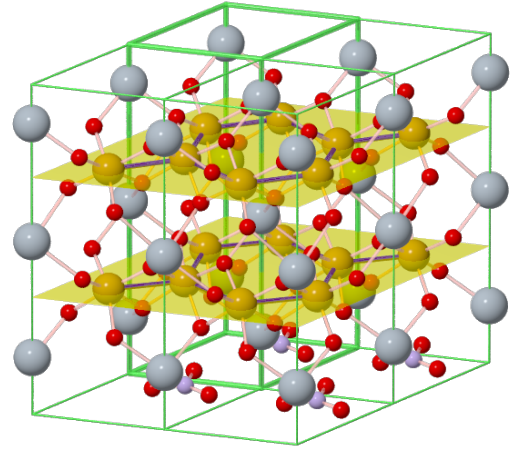


FIG. 1. (Color online) The 2×2 supercell of BMNO. The thicker green lines show the primitive cell. Two (yellow transparent) planes show honeycomb lattices which made of Mn atoms. In this figure, gray, red, yellow and violet spheres indicate Bi, O, Mn and N atoms.

(PAW) method, using Quantum-Espresso (QE) distribution [14]. To account for exchange-correlation interaction we use PBE functional [15] from Generalized Gradient Approximation (GGA). To improve estimation of electron-electron Coulomb interactions, we also add Hubbard-like U correction to DFT calculations, i.e., DFT+ U [16, 17].

To implement DFT+ U , FPLO uses Liechtenstein's approach [18, 19]. In Liechtenstein's approach the two parameters, U (on-site Coulomb repulsion) and J_H (the on-site Hund exchange) needs to be set, which we use $J_H = 1.0$ eV and $U = 1.5, 2.0, 3.0$ and 4.0 eV.

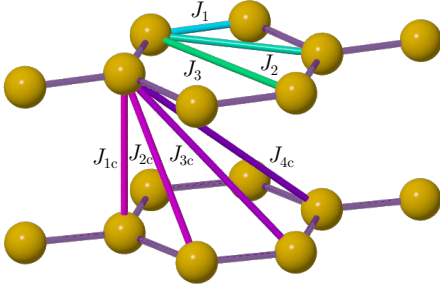


FIG. 2. J_1 , J_2 and J_3 indicate the Heisenberg exchange coupling constants between first, second and third nearest neighbor in-plane Mn^{+4} ions, respectively. J_{1c} , J_{2c} , J_{3c} and J_{4c} indicate the Heisenberg exchange coupling constants between inter-plane first, second and third nearest neighbor Mn^{+4} ions, respectively.

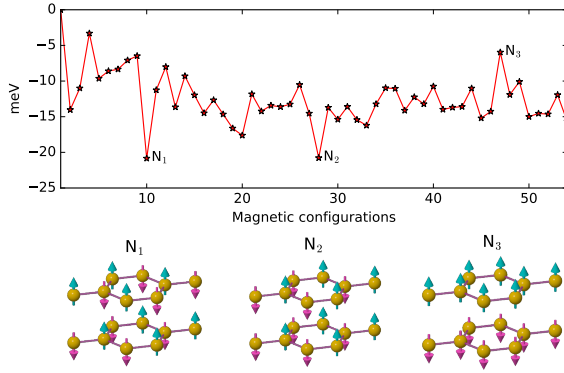


FIG. 3. (Color online) **(top)**: The ab initio energy landscape of 54 magnetic configurations obtained by DFT+ U with $U = 1.5$ eV. The energies of magnetic configurations are respect to fully ferromagnetic state whose energy is set to 0. **(bottom)**: Three magnetic configurations N_1 , N_2 and N_3 .

Spin Hamiltonian. The strategy of finding an effective spin Hamiltonian from ab initio calculations is to first compute the ground state energy for some given magnetic configurations. Then, mapping the energy difference of these configurations to an appropriate spin model gives us the coupling constants of the model. In this work, we use non-relativistic DFT, hence any magnetic anisotropy originating from the spin-orbit interaction is ignored in this approximation. Therefore, to leading order, we propose a spin Hamiltonian containing only bi-linear Heisenberg interactions, $\mathcal{H}_{\text{Heisenberg}} = \sum_{i>j} J_{ij} \mathbf{n}_i \cdot \mathbf{n}_j$, where \mathbf{n}_i and \mathbf{n}_j are classical unit vectors representing the orientation of the magnetic moments at sites i and j , respectively, with exchange interactions J_{ij} between them.

The primitive cell of $\text{Bi}_3\text{Mn}_4\text{O}_{12}(\text{NO}_3)$ contains 23 atoms. Because of the limitation in computational resources, we use the 2×2 supercell containing 92 atoms

(Fig. 1). This lets us to calculate J_{ij} 's up to the third nearest neighbors in-plane (J_1 , J_2 and J_3) and up to the fourth nearest neighbors inter-plane couplings (J_{1c} , J_{2c} , J_{3c} and J_{4c}) (see figure 2).

BMNO is metallic in GGA, however implementing spin-polarized calculation makes this compound insulating, independent of its magnetic configuration. Within co-linear spin polarized GGA, the ground state is a Néel state in which the nearest neighbor Mn magnetic moments (in and out of plane) are anti-parallel with respect to each other. This magnetic configuration is marked by N_1 in Fig. 3.

We calculated the total energy for more than 50 independent magnetic configurations. Then employing the least square method, enables us to obtain the exchange couplings with the accuracy of 0.02 meV. The top panel of figure 3 represents the energy landscape calculated for 54 different magnetic configurations within the super-cell shown in Fig. 1. The detailed description of these configurations is given in Ref.[20]. As it is obvious from this figure, the two configurations N_1 and N_2 (bottom panel of Fig. 3) are very close in energy space. In configuration N_2 , the magnetic ordering in each honeycomb layer is Néel type, but unlike N_1 , the magnetic moment orientations of two layer are parallel.

The coupling constants of the Heisenberg Hamiltonian, obtained by different values of on-site Coulomb interaction U , are given in Table. I. It is important to mention that to achieve equal couplings between equivalent Mn ions in the two layers, we need to geometrically optimize the atomic positions rather than just using the experimental atomic positions (for the details see supplementary information [20]).

The Mn spin state. The bond valence sum indicates the valence state $\text{Bi}_3^{3+}\text{Mn}_4^{4+}\text{O}_{12}^{2-}(\text{NO}_3)^-$ for BMNO [1]. However, using the charge analyzing code Critic2 [21, 22], within GGA/PAW, we find the valence state $\text{Bi}_3^{1.96+}\text{Mn}_4^{1.87+}\text{O}_{12}^{1.04-}(\text{NO}_3)^{0.86-}$ in N_1 -configuration. This charge distribution will not change dramatically in the case of implementing DFT+ U even with large U parameter. The local density analysis (Lowdin charges), also proposes the charge distribution $\text{Bi}_3^{1.49+}\text{Mn}_4^{1.45+}\text{O}_{12}^{0.74-}(\text{NO}_3)^{0.40-}$. These charge analyses show that the Mn-O bonds are ionic-covalent instead of being completely ionic. Indeed, the reason for such a fractional charge distribution in BMNO is the strong hybridization between Mn d-orbitals and the neighboring O p-orbitals. This also lowers the magnetic moment of Mn ions from $3\mu_B$ to about $2.5\mu_B$ (see Table.I in supplementary information [20]).

Monte Carlo Simulations. To gain insight into the finite temperature properties of the model hamiltonian, we perform MC simulation. MC simulations is done on a $24 \times 24 \times 1$ supercell contains 2304 Mn atoms with periodic boundary conditions. We use single spin Metropolis updating, 3×10^6 MC steps for thermalization and 7×10^6

TABLE I. Heisenberg constants obtained by ab initio calculations (LDA+ U) using different U and different methods. The geometrically optimized structure (in the ferromagnetic state) is used in these calculations. The last column shows Curie-Weiss temperature obtained from Monte Carlo simulations for a system size with $N = 4 \times 24 \times 24 \times 1$. The experimental Curie-Weiss temperature is between -257K [1] and -222K [2]. For comparison we also indicate the results from Ref. [5].

method	$U(\text{eV})$	$J_1(\text{meV})$	$J_2(\text{meV})$	$J_3(\text{meV})$	$J_{1c}(\text{meV})$	$J_{2c}(\text{meV})$	$J_{3c}(\text{meV})$	$J_{4c}(\text{meV})$	$\Theta_{CW}(K)$
FPLO	1.5	10.7	0.9	1.2	3.0	1.1	0.5	0.9	-244
	2.0	9.0	0.8	1.0	2.6	0.9	0.5	0.8	-203
	3.0	6.6	0.6	0.8	2.1	0.7	0.3	0.6	-144
	4.0	5.1	0.5	0.6	1.7	0.6	0.3	0.5	-111

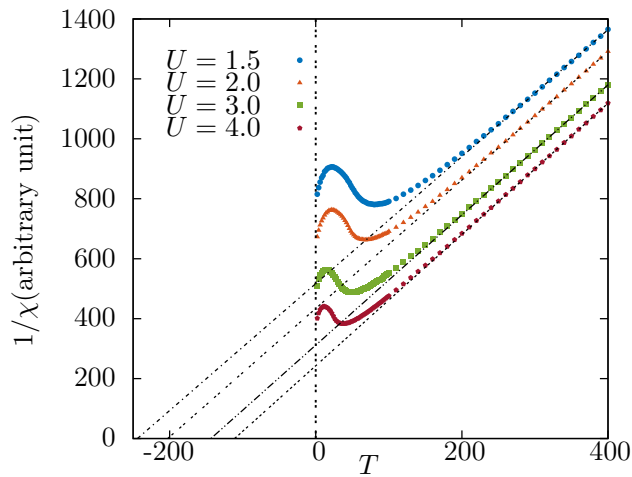


FIG. 4. (Color online) Temperature dependence of the inverse DC magnetic susceptibility ($1/\chi$) of BMNO obtained by MC simulations for different set of ab initio exchange couplings derived by using $U = 1.5$ eV (circles), $U = 2.0$ eV (triangles), $U = 3.0$ eV (squares) and $U = 4.0$ eV (pentagons). The crossing of the line fitted at high temperatures to $1/\chi$ with the horizontal axis gives the Curie-Weiss temperature.

MC samplings for the measurement of physical quantity. To reduce the correlations, we skip 5 MC sweeps between successive data collections.

Figure 4 represents the inverse of magnetic susceptibility per unit cell versus temperature for two sets of exchange couplings obtained by ab initio method using $U = 1.5, 2.0, 3.0$ and $U = 4.0$ eV. The linear fit at high temperatures crosses the T -axis at a negative value which is the Curie-Weiss temperature θ_{CW} . It can be seen that θ_{CW} increases by increasing the value of onsite coulomb repulsion U . The $\theta_{CW} = -244\text{K}$ is closest to what has been measured experimentally.

To speculate about the ground state of the Hamiltonian, we calculated the inter-layer spin-spin correlation at a low temperature, up to forth neighbors (Fig. 5). The correlations are calculated by averaging over 5×10^4 MC samplings at $T = 2\text{K}$. As it can be seen from this figure, for the couplings corresponding to $U = 1.5$ eV (Table. I), the spin-spin correlations between the two layers are

very small. However, increasing (decreasing) the value of J_{2c} by only 5 percent, while keeping the rest of the couplings unchanged, pushes the system toward N_1 (N_2) type ordering.

Quantum effects. To make an inquiry about the quantum correlations at zero temperature, we use the density matrix renormalization group (DMRG) techniques based on a matrix product state representation to evaluate the spin correlations functions [23]. In our calculations, we consider a lattice with $2 \times 5 \times 5$ sites. The spin-spin correlations normalized by S^2 (shown in the bottom panel of Fig. 5), confirms the transition from N_1 to N_2 states at $J_{2c}/J_1 \sim 0.1$, despite the weakening of the correlations as the effect of quantum fluctuations. This is while, the in-plane spins are in the Néel state, independent of the value of J_{2c} (Fig. 6).

Conclusion. In summary, we employed an ab initio LDA+ U method to obtain the exchange coupling constants of a spin Hamiltonian for describing the magnetic properties of the honeycomb bilayer BMNO and figure

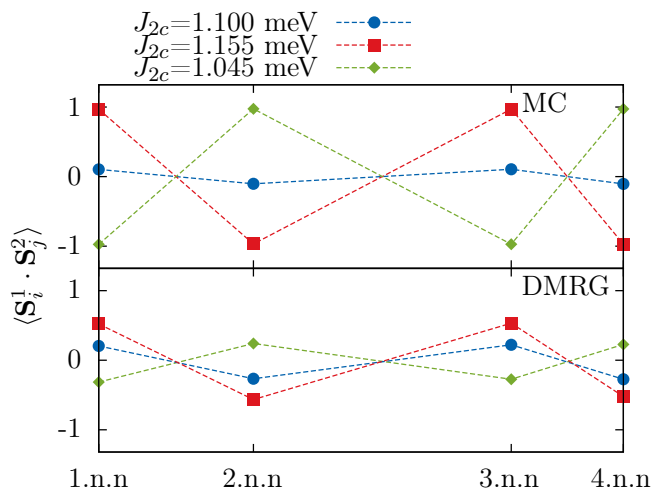


FIG. 5. (Color online) Interlayer spin-spin correlation up to forth neighbor obtain by (top) MC simulation, (bottom) DMRG (normalized by S^2). $J_1, J_2, J_3, J_{1c}, J_{3c}$ and J_{4c} are kept fixed at those found by $U = 1.5$ eV. The spin-spin correlations at $J_{2c} = 1.100$ meV are obtained by using $U = 1.5$ eV and compared with $J_{2c} = 1.045$ and $J_{2c} = 1.155$ meV.

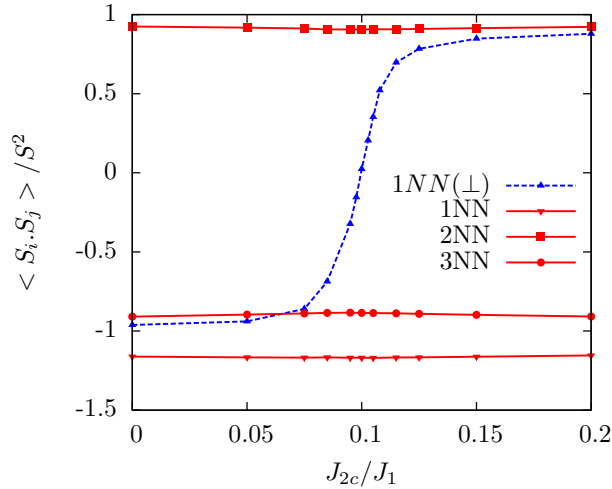


FIG. 6. (Color online) DMRG results for the variation of spin-spin correlations for first, second, third in-plane neighbors and first inter-plane neighbors versus J_{2c}/J_1 . Other coupling are fixed by those obtained by $U = 1.5$ eV (first row of the Table I)

out the reason that this compound does not show any ordering down to very low temperatures. Using $U = 1.5$ eV, we found that a Hamiltonian containing only bilinear Heisenberg terms up to third in-plane and fourth out of plane nearest neighbor, well matches the measured DC magnetic susceptibility for this material.

Classical MC simulations and DMRG calculations on this spin Hamiltonian shows no sign of long-range ordering down to zero temperature. We found that the coupling having the major effect on the frustration of the Hamiltonian is the second inter-plane exchange J_{2c} . Indeed, in BMNO the ratio $J_{2c}/J_1 \sim 0.1$ is fine tuned to be close to the transition point of the two collinear configurations N_1 and N_2 . At this very special point, the spin-spin correlations in each layer are Néel type, however, there is almost a vanishing correlation between the two layers, making the dynamics of the two Néel states uncorrelated. The lack of correlations between the adjacent layer makes BMNO an effectively two-dimensional Heisenberg system for which there would be no finite temperature phase transition, according to the Mermin-Wagner theorem. We also speculate that the quantum ground state of BMNO is a linear superposition of the two types of Néel configurations N_1 and N_2 which could give rise to a quantum spin liquid state for this compound. Verification of this speculation requires further investigations.

We acknowledge Michel Gingras, Jeff Rau and Stefano de Gironcoli for the most useful discussions and comments. We also thank Phivos Mavropoulos for providing us with his MC code.

- * m.alaei@cc.iut.ac.ir
† shahbazi@cc.iut.ac.ir
- [1] O. Smirnova, M. Azuma, N. Kumada, Y. Kusano, M. Matsuda, Y. Shimakawa, T. Takei, Y. Yonesaki, and N. Kinomura, *Journal of the American Chemical Society* **131**, 8313 (2009).
 - [2] N. Onishi, K. Oka, M. Azuma, Y. Shimakawa, Y. Motome, T. Taniguchi, M. Hiraishi, M. Miyazaki, T. Masuda, A. Koda, *et al.*, *Physical Review B* **85**, 184412 (2012).
 - [3] M. Matsuda, M. Azuma, M. Tokunaga, Y. Shimakawa, and N. Kumada, *Phys. Rev. Lett.* **105**, 187201 (2010).
 - [4] S. Okubo, F. Elmasry, W. Zhang, M. Fujisawa, T. Sakurai, H. Ohta, M. Azuma, O. A. Sumirnova, and N. Kumada, *Journal of Physics: Conference Series* **200**, 022042 (2010).
 - [5] H. C. Kandpal and J. van den Brink, *Physical Review B* **83**, 140412 (2011).
 - [6] R. Ganesh, D. Sheng, Y.-J. Kim, and A. Paramekanti, *Physical Review B* **83**, 144414 (2011).
 - [7] R. Ganesh, S. V. Isakov, and A. Paramekanti, *Physical Review B* **84**, 214412 (2011).
 - [8] J. Oitmaa and R. Singh, *Physical Review B* **85**, 014428 (2012).
 - [9] S. Okubo, T. Ueda, H. Ohta, W. Zhang, T. Sakurai, N. Onishi, M. Azuma, Y. Shimakawa, H. Nakano, and T. Sakai, *Phys. Rev. B* **86**, 140401 (2012).
 - [10] H. Zhang, M. Arlego, and C. Lamas, *Physical Review B* **89**, 024403 (2014).
 - [11] F. G. Albarracín and H. Rosales, *Physical Review B* **93**, 144413 (2016).
 - [12] R. Bishop and P. Li, arXiv preprint arXiv:1611.03287 (2016).
 - [13] K. Koepnik and H. Eschrig, *Phys. Rev. B* **59**, 1743 (1999).
 - [14] P. Giannozzi, S. Baroni, N. Bonini, M. Calandra, R. Car, C. Cavazzoni, D. Ceresoli, G. L. Chiarotti, M. Cococcioni, I. Dabo, A. D. Corso, S. de Gironcoli, S. Fabris, G. Fratesi, R. Gebauer, U. Gerstmann, C. Gougoussis, A. Kokalj, M. Lazzeri, L. Martin-Samos, N. Marzari, F. Mauri, R. Mazzarello, S. Paolini, A. Pasquarello, L. Paulatto, C. Sbraccia, S. Scandolo, G. Sclauszero, A. P. Seitsonen, A. Smogunov, P. Umari, and R. M. Wentzcovitch, *Journal of Physics: Condensed Matter* **21**, 395502 (2009).
 - [15] J. P. Perdew, K. Burke, and M. Ernzerhof, *Phys. Rev. Lett.* **77**, 3865 (1996).
 - [16] V. I. Anisimov, J. Zaanen, and O. K. Andersen, *Phys. Rev. B* **44**, 943 (1991).
 - [17] V. I. Anisimov, I. V. Solovyev, M. A. Korotin, M. T. Czyżyk, and G. A. Sawatzky, *Phys. Rev. B* **48**, 16929 (1993).
 - [18] A. I. Liechtenstein, V. I. Anisimov, and J. Zaanen, *Phys. Rev. B* **52**, R5467 (1995).
 - [19] H. Eschrig, K. Koepnik, and I. Chaplygin, *Journal of Solid State Chemistry* **176**, 482 (2003), special issue on The Impact of Theoretical Methods on Solid-State Chemistry.
 - [20] See Supplementary Material.
 - [21] A. O. de-la Roza, E. R. Johnson, and V. Luaa, *Computer Physics Communications* **185**, 1007 (2014).

- [22] A. O. de-la Roza, M. Blanco, A. M. Pends, and V. Luaa, *Computer Physics Communications* **180**, 157 (2009).
 [23] M. Dolfi, B. Bauer, S. Keller, A. Kosenkov, T. Ewart, A. Kantian, T. Giamarchi, and M. Troyer, *Computer Physics Communications* **185**, 3430 (2014).

SUPPLEMENTAL MATERIAL

CHARGE ANALYSIS

In this section, we explain why Mn-O bonds has ionic-covalent character. In fact, the ionic-covalent character of Mn-O bonds can be observed in the hybridization of Mn- d and O- p orbitals. The point group of MnO_6 clusters in $\text{Bi}_3\text{Mn}_4\text{O}_{12}(\text{NO}_3)$ is C_3 , where the C_3 -axis is perpendicular to honeycomb layer. Therefore, the Mn- d orbitals are splitted as the effect of the crystal field into d_{z^2} , (d_{xz}, d_{yz}) and $(d_{xy}, d_{x^2-y^2})$. The projected density of states plotted in figure 7 together with the orbital occupation calculation shown in Table. II, indicate that the hybridization among d orbitals of Mn and p orbitals of O makes the crystal field states (d_{xz}, d_{yz}) and $(d_{xy}, d_{x^2-y^2})$ to have fractional occupations. Therefore the bond va-

TABLE II. Charge distribution among Mn- d orbitals obtained by GGA/PAW Lowdin charge analysis.

spin	d_{tot}	d_{z^2}	(d_{xz}, d_{yz})	$(d_{xy}, d_{x^2-y^2})$
\uparrow	3.8456	0.9825	0.6296	0.8020
\downarrow	1.2960	0.1890	0.2914	0.2621

lence sums $(\text{Bi}_3^{3+}\text{Mn}_4^{4+}\text{O}_{12}^{2-}(\text{NO}_3)^-)$ [1] does not give rise to a true understanding of the charge distribution and also about magnetization of Mn atoms.

Figure 7 also shows a wide range of PDOS for all occupied d -orbitals, which could be a reason that why the onsite electron-electron repulsion parameter U is not very large in this system.

EXCHANGE CONSTANTS

In the experimental structure of $\text{Bi}_3\text{Mn}_4\text{O}_{12}(\text{NO}_3)$ [1] (with $P3$ space group), There is a small difference between vertical positions of Mn atoms in the unit cell. The Wyckoff positions of the four Mn atoms are as: Mn_1 $2/3$ $1/3$ $0.855(5)$, Mn_2 $1/3$ $2/3$ $0.852(6)$, Mn_3 $2/3$ $1/3$ $0.218(5)$, Mn_4 $1/3$ $2/3$ $0.223(6)$. In the DFT calculations, we found that Mn_1 and Mn_2 as well as Mn_3 and Mn_4 do not have the same vertical positions, even if exact geometry optimization is performed. Since Mn atoms are not completely identical, we have to use more Heisenberg constants. For example, instead of only one J_1 for

first nearest neighbor interaction we need to consider two: one between Mn_1 and Mn_2 ($J_1^{1,2}$) and the other between

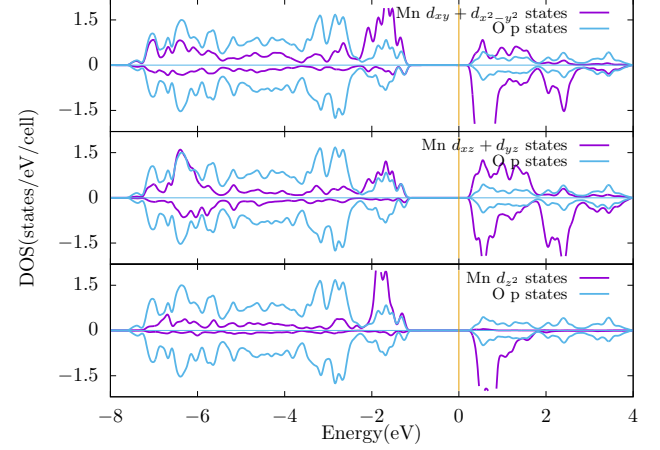


FIG. 7. Projected Density of States (PDOS) of Mn- d and O- p orbitals.

Mn_3 and Mn_4 ($J_1^{3,4}$). For the second neighbor couplings J_2 we also have $J_2^{1,1}$, $J_2^{2,2}$, $J_2^{3,3}$ and $J_2^{4,4}$. Similarly, there are variety of couplings for other inter and intra layer exchange interactions (see Table. III).

To calculate the couplings of the Heisenberg Hamiltonian, we use 54 magnetic configurations listed in Table. V. Employing the least square method by considering these 54 magnetic configurations, enables us to calculate the magnetic exchanges the within accuracy of 0.02 meV.

The ab initio results for the exchange couplings are given in Table. III. These results are obtained after performing geometry optimization in a ferromagnetic configuration. The differences between the couplings of the same range are small ($\sim 0.1\text{meV}$), hence their arithmetic mean are reported in the main paper.

Using the experimental structure, the difference between the couplings of the same range are significant (see Table IV). For example, $J_1^{1,2}=27.4\text{ meV}$ $J_1^{3,4}=10.8\text{ meV}$ within GGA/FPLO method. So the assumption of identical Mn atoms in the experimental structure for derivation of J_{ij} is not correct.

MAGNETIC CONFIGURATIONS

In this section, we show the 54 magnetic configurations used for the calculations of the Heisenberg coupling constants. To represent magnetic configurations, we assign a number on each Mn atoms in the $2 \times 2 \times 1$ supercell of $\text{Bi}_3\text{Mn}_4\text{O}_{12}(\text{NO}_3)$ (figure 8), and then we specify the direction of Mn magnetic moments (up or down) by arrows shown in Table. V.

TABLE III. Heisenberg constants obtained by ab initio calculations (LDA+ U) using FPLO. The structure, which is used in these calculations, is derived from geometry optimization of $\text{Bi}_3\text{Mn}_4\text{O}_{12}(\text{NO}_3)$ in its ferromagnetic state.

method	U	$J_1^{1,2}$	$J_1^{3,4}$	$J_2^{1,1}$	$J_2^{2,2}$	$J_2^{3,3}$	$J_2^{4,4}$	$J_3^{(1,2)}$	$J_3^{3,4}$	$J_{1c}^{1,3}$	$J_{1c}^{2,4}$	$J_{2c}^{1,3}$	$J_{2c}^{2,4}$	$J_{3c}^{1,3}$	$J_{3c}^{2,4}$	$J_{4c}^{1,3}$	$J_{4c}^{2,4}$
FPLO	1.5	10.8	10.7	1.0	0.8	1.0	0.8	1.2	1.2	2.9	3.0	1.1	1.1	0.5	0.6	0.9	0.9
	2.0	9.0	9.0	0.9	0.7	0.9	0.7	1.0	1.0	2.6	2.6	1.0	0.9	0.4	0.5	0.8	0.8
	3.0	6.6	6.6	0.7	0.6	0.7	0.6	0.8	0.8	2.0	2.1	0.7	0.7	0.3	0.4	0.6	0.6
	4.0	5.1	5.1	0.5	0.4	0.5	0.5	0.6	0.7	1.6	1.7	0.6	0.6	0.3	0.3	0.5	0.5

TABLE IV. Heisenberg constants obtained by ab initio calculations (LDA+ U) using different U and different methods. The experimental structure is used in these calculations.

method	U	$J_1^{1,2}$	$J_1^{3,4}$	$J_2^{1,1}$	$J_2^{2,2}$	$J_2^{3,3}$	$J_2^{4,4}$	$J_3^{1,2}$	$J_3^{3,4}$	$J_{1c}^{1,3}$	$J_{1c}^{2,4}$	$J_{2c}^{1,3}$	$J_{2c}^{2,4}$	$J_{3c}^{1,3}$	$J_{3c}^{2,4}$	$J_{4c}^{1,3}$	$J_{4c}^{2,4}$
FPLO	0.0	27.4	10.8	0.9	0.7	2.5	2.0	1.2	2.2	4.6	5.9	1.8	1.3	0.2	0.6	1.0	0.7
	2.0	18.4	6.5	0.6	0.5	1.6	1.4	0.8	1.3	2.7	3.6	1.2	1.0	0.3	0.6	0.9	0.7
	3.0	14.1	4.3	0.5	0.4	1.2	1.1	0.6	1.0	2.2	2.8	0.9	0.8	0.3	0.4	0.7	0.5
	4.0	11.1	2.8	0.3	0.3	1.0	0.8	0.5	0.8	1.7	2.3	0.7	0.6	0.2	0.3	0.5	0.4

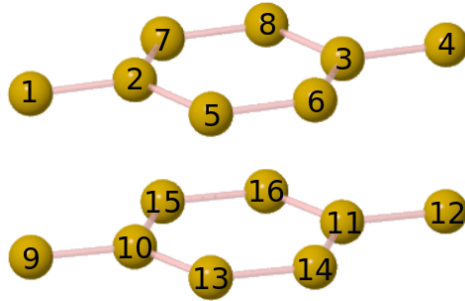


FIG. 8. Each Mn atoms are labeled by a number in $2 \times 2 \times 1$ supercell of $\text{Bi}_3\text{Mn}_4\text{O}_{12}(\text{NO}_3)$

TABLE V. 54 magnetic configurations which are used to derive J_{ij} .

Magnetic configuration	Mn ₁	Mn ₂	Mn ₃	Mn ₄	Mn ₅	Mn ₆	Mn ₇	Mn ₈	Mn ₉	Mn ₁₀	Mn ₁₁	Mn ₁₂	Mn ₁₃	Mn ₁₄	Mn ₁₅	Mn ₁₆
1	↑	↑	↑	↑	↑	↑	↑	↑	↑	↑	↑	↑	↑	↑	↑	↑
2	↑	↑	↓	↓	↑	↓	↑	↓	↑	↑	↓	↓	↑	↓	↑	↓
3	↑	↓	↓	↑	↑	↑	↑	↑	↑	↓	↓	↑	↑	↑	↑	↑
4	↑	↓	↑	↑	↑	↑	↑	↑	↑	↑	↑	↑	↑	↑	↑	↑
5	↓	↓	↑	↑	↑	↑	↑	↑	↓	↓	↑	↑	↑	↑	↑	↑
6	↑	↑	↓	↓	↑	↓	↑	↓	↑	↑	↑	↑	↑	↑	↑	↑
7	↑	↑	↓	↓	↓	↓	↓	↓	↑	↑	↑	↑	↑	↑	↑	↑
8	↑	↓	↑	↑	↓	↑	↓	↓	↑	↑	↑	↑	↑	↑	↑	↑
9	↑	↑	↑	↑	↓	↑	↓	↑	↑	↑	↑	↑	↑	↑	↑	↑
10(N ₁)	↑	↓	↑	↓	↑	↓	↑	↓	↓	↑	↓	↑	↓	↑	↓	↑
11	↓	↓	↑	↑	↓	↓	↑	↑	↓	↓	↑	↑	↑	↑	↑	↑
12	↓	↓	↓	↑	↑	↑	↑	↑	↑	↑	↑	↑	↑	↑	↑	↑
13	↓	↓	↓	↑	↑	↑	↑	↑	↓	↓	↓	↑	↑	↑	↑	↑
14	↓	↓	↓	↓	↑	↑	↑	↑	↑	↑	↑	↑	↑	↑	↑	↑
15	↑	↓	↑	↓	↑	↓	↑	↓	↑	↑	↑	↑	↑	↑	↑	↑
16	↑	↑	↑	↑	↑	↓	↑	↓	↑	↓	↑	↑	↑	↑	↑	↑
17	↓	↓	↓	↓	↑	↑	↑	↑	↓	↓	↑	↑	↑	↑	↑	↑
18	↓	↓	↓	↓	↑	↑	↑	↑	↓	↓	↓	↓	↑	↑	↑	↑
19	↑	↓	↑	↓	↑	↓	↑	↓	↑	↓	↓	↑	↑	↑	↑	↑
20	↑	↓	↑	↓	↑	↓	↑	↓	↑	↓	↓	↓	↑	↑	↑	↑
21	↑	↓	↑	↑	↓	↑	↑	↓	↑	↓	↑	↑	↓	↑	↑	↑
22	↓	↓	↓	↓	↑	↑	↑	↑	↑	↑	↓	↑	↓	↑	↑	↑
23	↑	↑	↓	↓	↑	↑	↓	↑	↓	↑	↑	↓	↑	↑	↑	↓
24	↑	↑	↓	↑	↑	↑	↓	↑	↓	↑	↑	↓	↑	↑	↑	↓
25	↓	↑	↓	↓	↓	↓	↓	↓	↓	↑	↓	↑	↑	↑	↓	↑
26	↑	↑	↓	↑	↑	↓	↓	↑	↑	↑	↑	↑	↑	↑	↓	↑
27	↑	↑	↓	↓	↑	↓	↓	↑	↑	↑	↓	↑	↓	↑	↑	↓
28(N ₂)	↑	↓	↑	↓	↑	↓	↑	↓	↑	↓	↑	↓	↑	↓	↑	↓
29	↓	↓	↓	↓	↑	↓	↑	↓	↑	↑	↓	↑	↓	↑	↑	↑
30	↓	↓	↓	↑	↓	↑	↓	↑	↓	↓	↑	↓	↓	↑	↑	↑
31	↓	↑	↓	↑	↑	↑	↓	↑	↑	↓	↑	↑	↓	↓	↓	↑
32	↑	↑	↑	↑	↓	↓	↓	↑	↑	↑	↓	↑	↓	↑	↓	↑
33	↑	↑	↑	↓	↑	↓	↓	↓	↓	↑	↓	↓	↓	↑	↑	↑
34	↓	↓	↑	↓	↑	↑	↓	↓	↓	↓	↓	↑	↑	↓	↑	↑
35	↓	↑	↓	↓	↓	↑	↓	↓	↓	↓	↑	↑	↓	↓	↓	↓
36	↓	↑	↓	↓	↑	↑	↓	↓	↑	↑	↑	↑	↑	↑	↓	↑
37	↓	↓	↑	↑	↓	↓	↑	↓	↓	↑	↑	↑	↓	↑	↓	↓
38	↑	↑	↑	↓	↑	↑	↑	↓	↑	↑	↓	↓	↓	↑	↑	↑
39	↑	↓	↓	↑	↓	↓	↑	↓	↓	↓	↓	↓	↑	↑	↓	↓
40	↑	↓	↑	↑	↑	↑	↑	↑	↑	↓	↓	↓	↓	↑	↑	↑
41	↓	↑	↑	↑	↑	↓	↓	↓	↑	↓	↑	↓	↓	↓	↑	↑
42	↑	↑	↑	↓	↓	↓	↓	↓	↑	↑	↑	↑	↑	↓	↑	↓
43	↑	↑	↓	↓	↓	↓	↓	↑	↓	↓	↓	↓	↓	↑	↑	↑
44	↓	↑	↑	↑	↑	↑	↑	↑	↓	↓	↓	↑	↑	↑	↑	↓
45	↓	↑	↑	↓	↓	↑	↓	↓	↓	↓	↓	↓	↑	↑	↑	↑
46	↑	↑	↓	↓	↓	↓	↓	↑	↑	↑	↑	↓	↑	↓	↓	↑
47(N ₃)	↑	↑	↑	↑	↑	↑	↑	↑	↑	↓	↓	↓	↓	↓	↓	↓
48	↓	↓	↓	↓	↓	↓	↓	↑	↑	↑	↑	↑	↓	↓	↓	↑
49	↑	↓	↓	↓	↓	↑	↓	↓	↓	↓	↑	↓	↓	↓	↓	↑
50	↓	↓	↑	↓	↑	↑	↑	↓	↓	↓	↓	↑	↓	↑	↑	↓
51	↑	↑	↓	↑	↑	↓	↑	↓	↓	↑	↑	↓	↓	↑	↓	↑
52	↓	↑	↓	↓	↓	↓	↓	↑	↓	↑	↓	↑	↓	↑	↓	↓
53	↑	↑	↓	↑	↑	↓	↑	↑	↓	↓	↑	↑	↓	↓	↓	↑
54	↓	↑	↓	↑	↓	↑	↑	↑	↓	↓	↑	↑	↓	↑	↓	↑